gravitational effects. Additionally, the giant molecular cloud material that existed before the formation of the stars in the W3OH region could have been accelerated by shocks associated with supernovae in the region (*17*–*19*). Overall, it remains to be seen whether one can account for the peculiar motion of W3OH in the context of the spiral density-wave paradigm.

We have established that the VLBA can achieve a parallax accuracy of 0.01 mas and a proper motion accuracy of better than 1 km s^{-1} for Galactic sources with only five observations spanning 1 year. With this accuracy, the VLBA can be used to measure distances to 10 kpc with better than 10% accuracy, which is approximately a factor of 100 better than the Hipparcos satellite. Based on these results, we believe that the VLBA, and ultimately the Japanese Very Long Baseline Interferometric project VERA [VLBI Exploration of Radio Astrometry (*20*)], can map the spiral structure and full kinematics of massive star–forming regions in the Milky Way.

References and Notes

1. V. L. Fish, M. J. Reid, D. J. Wilner, E. Churchwell, *Astrophys. J.* **587**, 701 (2003).
2. Y. M. Georgelin, Y. P. Georgelin, *Astron. Astrophys.* **49**, 57 (1976).
3. J. H. Taylor, J. M. Cordes, *Astrophys. J.* **411**, 674 (1993).
4. R. M. Humphreys, *Astrophys. J.* **38** (supp.), 309 (1978).
5. The LSR is a reference frame at the position of the Sun and moving in a circle about the center of the Milky Way; in practice, this frame is determined from the average motion of large numbers of stars in the solar neighborhood.
6. F. J. Kerr, D. Lynden-Bell, *Mon. Not. R. Astron. Soc.* **221**, 1023 (1986).
7. M. A. C. Perryman *et al.*, *Astron. Astrophys.* **323**, L49 (1997).
8. K. M. Menten *et al.*, *Astrophys. J.* **333**, L83 (1988).
9. L. Moscadelli, K. M. Menten, C. M. Walmsley, M. J. Reid, *Astrophys. J.* **519**, 244 (1999).
10. The National Radio Astronomy Observatory is operated by Associated Universities Inc., under cooperative agreement with the U.S. National Science Foundation.
11. K. Hachisuka *et al.*, *Astrophys. J.*, in press.
12. The OH masers toward the methanol masers we detect are near the origin of the maps of (*21*).
13. D. R. H. Johnson, D. R. Soderblom, *Astron. J.* **93**, 864 (1987).
14. W. Dehnen, J. J. Binney, *Mon. Not. R. Astron. Soc.* **298**, 387 (1998).
15. C. C. Lin, C. Yuan, F. H. Shu, *Astrophys. J.* **155**, 721 (1969).
16. W. W. Roberts, *Astrophys. J.* **259**, 283 (1972).
17. B. Dennison, G. A. Topasna, J. H. Simonetti, *Astrophys. J.* **474**, L31 (1997).
18. R. J. Reynolds, N. C. Sterling, L. M. Haffner, *Astrophys. J.* **558**, L101 (2001).
19. M. S. Oey, A. M. Watson, K. Kern, G. L. Walth, *Astron. J.* **129**, 393 (2005).
20. M. Honma, N. Kawaguchi, T. Sasao, in *Proceedings of SPIE,* Vol. 4015, Radio Telescopes, H. R. Butcher, Ed. (SPIE–The International Society for Optical Engineering, Bellingham, WA, 2000), pp. 624–631.
21. E. E. Bloemhof, M. J. Reid, J. M. Moran, *Astrophys. J.* **397**, 500 (1992).

22. Y.X. and X.W.Z. thank the Smithsonian Institution for support through its visiting scientist program. Research on the structure of the Milky Way at Nanjing University is supported by the National Science Foundation of China under grants 10133020 and 10373025.

Supporting Online Material

www.sciencemag.org/cgi/content/full/1120914/DC1
SOM Text
Fig. S1
References

3 October 2005; accepted 16 November 2005
Published online 8 December 2005;
10.1126/science.1120914
Include this information when citing this paper.

Quantum Dynamics of a d-Wave Josephson Junction

Thilo Bauch,[1] Tobias Lindström,[1] Francesco Tafuri,[2] Giacomo Rotoli,[3] Per Delsing,[1] Tord Claeson,[1] Floriana Lombardi[1]*

Here we present the direct observation of macroscopic quantum properties in an all high-critical-temperature superconductor d-wave Josephson junction. Although dissipation caused by low-energy excitations is expected to strongly suppress macroscopic quantum effects, we demonstrate energy level quantization in our d-wave Josephson junction. The result indicates that the role of dissipation mechanisms in high-temperature superconductors has to be revised, and it may also have consequences for the class of solid-state "quiet" quantum bits with superior coherence time.

In terms of engineering quantum-information applications and searching for physical systems where quantum mechanics can be applied at a macroscopic level, superconductors have inherent advantages (*1*). Indeed, the detection of macroscopic quantum tunneling and energy-level quantization effects in conventional Josephson junction (JJ) circuits (*2*) has enabled the fabrication of superconductive quantum devices based on low–critical-temperature superconductor (LTS) Josephson junctions. The quantum superposition of distinct macroscopic states (*3*, *4*) and the observation of Rabi oscillations (*5*–*9*) have also been reported in these devices. Superconductive quantum devices take advantage of a well-developed gap in the excitation spectrum of quasiparticles, which favors less dissipation, and the coherence of the superconducting state helps to achieve sufficiently long phase-coherence times. First-principle design and operation of superconducting devices has been demonstrated, and simple quantum protocols now appear feasible (*1*, *10*). High–critical-temperature superconductors (HTSs) are another candidate for quantum circuitry because of a d-wave order-parameter symmetry (*11*), a property which favors a naturally bistable system (a qubit) working in a particular "quiet" configuration (*12*–*15*). The operating point of the qubit is protected from external field fluctuations already at the classical level (*15*). The interest in HTS quantum systems is not only limited to quantum circuitry design, but also addresses fundamental issues on the nature of superconductivity and dissipation and the coherence in such objects.

However, one of the main arguments against HTS qubits based on systems with d-wave order-parameter symmetry is the presence of low-energy excitations inducing dissipation (*11*, *16*–*18*), a property which is expected to prevent the occurrence of macroscopic quantum phenomena, which are the key element for qubits. Here we report the observation of energy-level quantization in d-wave JJ, a clear signature of macroscopic quantum behavior and an indication that the dissipation in a d-wave JJ is low enough to allow the formation of the "sharp" energy levels required for a qubit. The result also indicates that the role of dissipation mechanisms in HTSs has to be revised and that d-wave devices do possess a macroscopic quantum degree of freedom.

The dynamics of a current-biased JJ is well established for LTSs. Within the resistively and capacitively shunted junction (RCSJ) model (Fig. 1A) (*19*), the Josephson inductance L_J and capacitance C_J act as an anharmonic LC resonator (at zero voltage) with resonance frequency $\omega_P = (L_J C_J)^{-1/2}$. The Josephson inductance is given by $L_J = \varphi_0/2\pi I_c \cos\varphi$, where I_c is the critical current, φ is the phase difference across the junction, and $\varphi_0 = h/2e$ is the superconducting flux quantum, where h is Planck's constant and e is the charge of an electron. For bias currents I close to the critical current I_c, the junction potential $U(\varphi)$ can be approximated by a cubic potential (Fig. 1B). The phase may escape from the well either by thermal activation or by tunneling through the barrier potential, and it corresponds to the junction switching from the zero voltage state to a finite voltage state. The escape is dominated by tunneling (*20*) at low temperature. The quantum bound states formed in the well with energy E_n, where n indicates the nth energy level, are shown in Fig. 1B. Only the

[1]Quantum Device Physics Laboratory, Department of Microtechnology and Nanoscience, MC2, Chalmers University of Technology, S-412 96 Göteborg, Sweden. [2]Istituto Nazionale per la Fisica della Materia–Dipartimento Ingegneria dell'Informazione, Seconda Università di Napoli, Aversa (CE), Italy. [3]Dipartimento di Ingegneria Meccanica, Energetica e Gestionale, Università of L'Aquila, Località Monteluco, L'Aquila, Italy.

*To whom correspondence should be addressed. E-mail: floriana.lombardi@mc2.chalmers.se

ground state is populated at temperatures smaller than the energy-level separation. The quantum states can be observed spectroscopically by inducing a resonant transition between the ground state and excited states by applying microwaves at frequencies $\nu_{0n} = (E_n - E_0)/h$. The width of the first excited energy level is determined by the energy decay rate into the ground state, and is given by $1/\tau = \mathrm{Re}(Y)/C_J = \nu_{01}/Q$, where τ is the lifetime of the first excited level, $\mathrm{Re}(Y)$ is the real part of the frequency-dependent total shunting admittance Y causing dissipation, and Q is the quality factor of the junction (*21*).

We fabricated highly hysteretic (*22*), tunnel-like $YBa_2Cu_3O_{7-\delta}$ (YBCO) grain boundary JJs using the bi-epitaxial technique (*23*, *24*). Junctions were formed at the interface between a (103) YBCO film grown on a (110) $SrTiO_3$ (STO) substrate and a c-axis film deposited on a (110) CeO_2 seed layer. The orientation of the order parameter in the two electrodes is shown in Fig. 2A. In this experiment, we focused on JJs where a lobe of the order parameter of one electrode is facing a node in the other electrode. This configuration yields a natural double-degenerate ground state of interest for future qubit applications (*15*). The intrinsic sources of dissipation due to nodal quasiparticles and surface Andreev bound states are maximally enhanced.

The stray capacitance C_S of the electrodes, caused by the large dielectric constant of the STO substrate at low temperature (*25*) (dielectric constant $\varepsilon_r > 10{,}000$), and the kinetic inductance L_k, caused by c-axis transport in one of the electrodes, can be taken into account by a modified RCSJ model (Fig. 2, B and C). The energy-level separation in this simple model is given by $h\nu_{01} = (h/2\pi)[(L_J + L_k)C_S]^{-1/2}$ (*26*).

The enhancement of the escape rate is measured under microwave irradiation to detect the energy levels. This allows us to analyze the bias current dependence of the energy-level separation and determine the width of the first excited level, which gives information on the dissipation processes in the junction. By repeatedly ramping the bias current I from zero at a constant rate, we determined the switching current probability distribution $P(I)$ from the zero voltage state to the finite voltage state. This switching probability can be directly related to the escape rate $\Gamma(I)$ (*27*).

Microwaves at fixed frequency ν_{mw} were transmitted to the junction via a dipole antenna at a temperature below the cross over value, T_{cr}, separating the thermal and quantum regimes (*22*). When ν_{mw} of the incident radiation (or multiples of it) coincides with the bias current–dependent level separation of the junction, $\nu_{01}(I) = m\nu_{mw}$, the first excited state is populated (*28*). Here, m is an integer number corresponding to an m-photon transition from the ground state to the first excited state (Fig. 1B). Figure 3A shows the evolution of the switching-current histogram as a function of the applied microwave power for the three-photon process. At low power values (–20 dBm, measured at the room temperature termination), the occupation probability of the first excited state is negligible and the switching histogram is unperturbed, corresponding to the escape from the ground state. When the applied power is increased, the first excited state starts to be populated. Then the histogram becomes doubly peaked (–17 dBm and –16 dBm), corresponding to tunneling from the first excited and ground states. The occupation probability of the ground and first excited state will become comparable (50% each) by further increasing the applied power. The escape from the first excited state is exponentially faster and dominates. Therefore, the switching current distribution is again single peaked at –14 dBm.

The escape rates derived from the switching probabilities are shown for various microwave

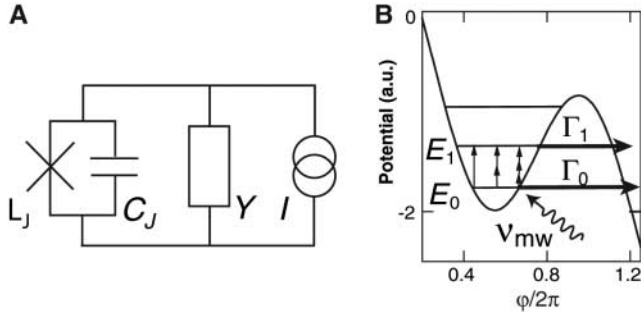

Fig. 1. Circuit diagram and energy levels. (**A**) Equivalent circuit diagram of a current-biased JJ. The Josephson inductance L_J and the junction capacitance C_J form an anharmonic oscillator. The damping of the oscillator caused by dissipation is described by the shunting admittance Y. It includes dissipation effects both intrinsic to the junction and caused by the electromagnetic environment connected through the biasing leads to the junction. (**B**) Energy levels in the cubic potential of the current-biased JJ. Microwave-induced transitions from the ground state (E_0) to the first excited state (E_1) are shown for the one-, two-, and three-photon processes. The phase tunnels out of the potential well at a rate Γ_0 from the ground state, and at a rate $\Gamma_1 \gg \Gamma_0$ from the first excited state that is populated by resonant microwave radiation. a.u., arbitrary units.

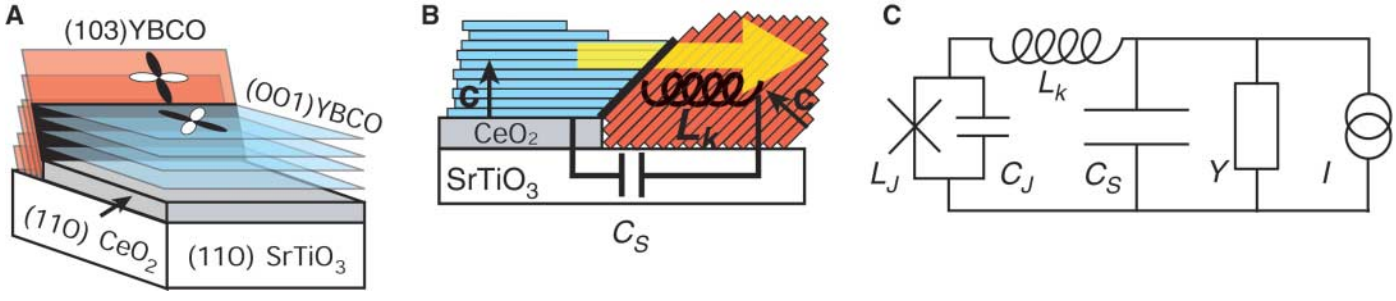

Fig. 2. Sample and extended circuit diagram. (**A**) Sketch of the bi-epitaxial YBCO junction. The JJ is formed at the boundary (black area) between (001) YBCO and (103) YBCO electrodes. A lobe of the superconducting order parameter in one electrode is facing a node of the order parameter in the other electrode. The normal state resistance of the JJ extracted from the current voltage characteristic is 450 ohms. The width w of the junction is 4 μm and the thickness t is 120 nm. The 4-μm-wide electrodes on both sides of the grain boundary extend over a length of 10 μm. 100-μm-wide leads then connect the electrodes to the bonding pads. (**B**) Cross section of the grain boundary junction. It illustrates the stray capacitance and kinetic inductance of the JJ. The large dielectric constant of the STO substrate at low temperature ($\varepsilon_r > 10{,}000$) results in a stray capacitance C_S between the electrodes dominating the total capacitance of the system. The large London penetration depth λ_L in the c-axis direction of the YBCO results in a large kinetic inductance L_k of one of the electrodes, where the bias current (yellow arrow) is partially flowing in the c direction. (**C**) Extended circuit diagram for the JJ, including the stray capacitance and kinetic inductance. The stray capacitance C_S can be considered in parallel to the junction through the electrode kinetic inductance L_k. For $C_S \gg C_J$, the stray inductance L_k adds up to the Josephson inductance L_J, resulting in an energy-level separation between the first excited state and ground state of our system given by the relation $h\nu_{01} = (h/2\pi)[(L_J + L_k)C_S]^{-1/2}$.

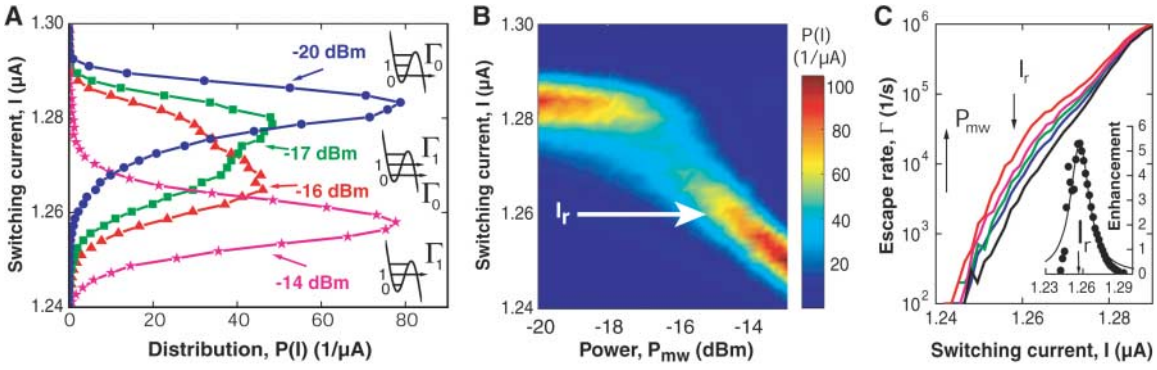

Fig. 3. Spectroscopy data. (**A**) Measured switching current probability distribution $P(I)$ in presence of microwaves at a frequency ν_{mw} = 850 MHz and temperature T = 15 mK. The applied power at the room temperature termination varies from −20 to −14 dBm. (**B**) Density plot of the measured $P(I)$ distributions as a function of the applied microwave power for ν_{mw} = 850 MHz and T = 15 mK. The resonance current I_r, where a resonant transition from the ground state to the first excited state occurs, is indicated by the arrow. (**C**) Escape rate extracted from the measured $P(I)$ distributions shown in Fig. 3A for increasing microwave power from −20 to −16 dBm (upward-pointing arrow). The escape rate is enhanced at the resonance current because of population of the first excited state. The enhancement of the escape rate $[\Gamma(P_{mw}) - \Gamma(0)]/\Gamma(0)$ at P_{mw} = −17 dBm is shown (solid circles) in the inset. The solid line is a fit to a Lorentzian. From the full width at half maximum, we extract a width in frequency $\delta\nu \approx 21$ MHz, yielding a quality factor $Q = \nu_{mw}/\delta\nu \approx 40$. The resonance current I_r is indicated by the downward-pointing arrows.

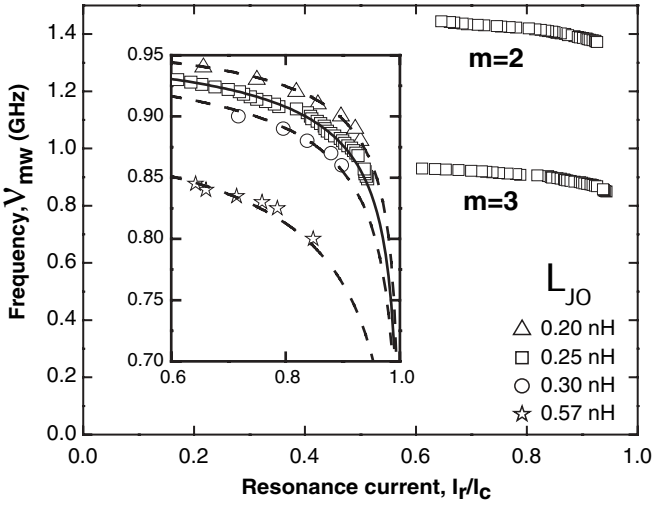

Fig. 4. Microwave frequency ν_{mw} versus normalized resonance current I_r/I_c. The two branches correspond to the two-photon (m = 2) and three-photon (m = 3) transitions. The ratio between the two- and three-photon frequencies is 3/2 within 3% for the measured range of resonant currents. The inset shows the measured microwave frequency versus normalized resonant current for the three-photon transition (m = 3) at four different Josephson inductances L_{J0} (symbols). The solid line is a fit to the experimental data with L_{J0} = 0.25 nH according to the resonance condition $6\pi\nu_{mw}(I_r) = C_S^{-1/2}[L_k + \varphi_o[1 - (I_r/I_c)^2]^{-1/2}/2\pi I_c]^{-1/2}$. The resulting fitting parameters L_k = 1.7 nH and C_S = 1.6 pF are used to calculate the frequency versus resonance current dependence for the other three values of the Josephson inductances (dashed lines). Experimentally, the families of values are obtained by varying the Josephson current by a magnetic field.

powers (Fig. 3C). A pronounced bump appears when the power is increased, indicating resonant activation of the excited level. The enhancement of the escape rate can be obtained by subtracting the unperturbed rate from the escape rate in the presence of microwaves (Fig. 3C, inset). The curve can be fitted by a Lorentzian, which indicates a resonant activation mechanism induced by level quantization. Moreover, the width of the enhancement curve is a measure of the quality factor Q. In the specific case of Fig. 3C, we get a Q value of the order of 40, which is comparable with the best results obtained in LTS junctions (*29*). However, much higher values for Q have been measured in LTS JJs by proper high-frequency engineering of the junction environment (*30*). The value of the quality factor demonstrates clearly that the dissipation mechanisms, including the one caused by low-energy excitations, do not prevent the observation of level quantization in the washboard potential.

The resonant bias current I_r, corresponding to the escape of the phase enhanced by microwaves (Fig. 3, B and C, arrow), is shown in Fig. 4 for various applied microwave frequencies. We can clearly distinguish two branches, corresponding to the two-photon (m = 2) and three-photon (m = 3) transitions from the ground state to the first excited state. The applicability of the equivalent circuit of Fig. 2C can be demonstrated by varying the Josephson inductance at zero bias, $L_{J0} = \varphi_0/2\pi I_c$, by an external magnetic field and measuring the bias current dependence of the energy-level separation ν_{01} for the three-photon process. The Josephson inductance L_{J0} at zero bias was determined from the unperturbed switching current histograms. From the fit of the data with L_{J0} = 0.25 nH (solid line in the inset of Fig. 4), we obtain the two fitting parameters: C_S = 1.6 pF and L_k = 1.7 nH. The dashed lines in the inset of Fig. 4 are the calculated current dependences of the three-photon transition frequencies from the ground to the first excited state using the same fitting parameters, C_S and L_k. The agreement between the experimental data and the calculated curves is excellent, indicating that the circuit of Fig. 2C describes well the Josephson quantum dynamics of our system. The fitted kinetic inductance agrees well with an estimate from geometry, $L_k = \mu_o\lambda_L^2/wt$, where μ_o is the magnetic constant, w is the width, and t is the thickness of the electrode, assuming an electrode length L = 10 μm and a London penetration depth in the c-axis direction $\lambda_L \approx 6$ μm (*31*). The correction to the Josephson inductance due to the doubly degenerate ground state can be neglected because of the large value of the kinetic inductance (*22*).

One may ask why no m = 1 curve is seen. We attribute the fact that we do not observe the one-photon (m = 1) transition at $\nu_{01} \approx 2.6$ GHz to the strongly frequency-dependent coupling of microwaves to the sample caused by the high dielectric constant of the STO substrate. Indeed, for frequencies larger than 4 GHz, no microwaves could be coupled; moreover, the STO substrate acts as a dielectric resonator. Therefore, microwaves can couple to the junction only at certain frequencies determined by the geometric resonance condition of the dielectric resonator. Microwaves that do not match the resonance condition of the STO substrate will be reflected to a large extent. This

seems to be the case for the one-photon transition frequency ν_{01}. This fact is also confirmed by the large quality factor that we extract from the resonant activation measurements. From Q, we derive the total shunting impedance $1/\mathrm{Re}(Y) = 4700$ ohms of the junction. This is much larger than the expected shunt impedance for a current-biased JJ, which is approximately the typical wire impedance at microwave frequencies ≈100 ohms. In this sense, the STO dielectric resonator protects the junction from its environment at the characteristic transition frequency ν_{01}.

Even though with our experiment, we are not able to determine univocally the intrinsic dissipation of the Josephson element, we can extract a lower bound. Assuming that all dissipation comes from the Josephson element, we can calculate the intrinsic impedance $1/\mathrm{Re}(Y_{\mathrm{int}})$ in parallel with the Josephson inductance. According to the circuit of Fig. 2C, we have $1/\mathrm{Re}(Y_{\mathrm{int}}) = L_J^2/(L_J + L_S)^2\mathrm{Re}(Y) \approx 700$ ohms for the lowest value of the intrinsic impedance due to low-lying energy excitations. This result may open up the possibility for some kind of freezing mechanism for quasiparticles at very low temperature and/or the existence of a subdominant imaginary s-wave component of the order parameter inducing a gapped excitation spectrum. The observation of quantum tunneling, narrow width of excited states, and a large Q value support the notion of "quiet" qubits based on d-wave symmetry superconductor.

References and Notes

1. Y. Makhlin, G. Schön, A. Shnirman, *Rev. Mod. Phys.* **73**, 357 (2001).
2. J. Clarke, A. N. Cleland, M. H. Devoret, D. Esteve, J. M. Martinis, *Science* **239**, 992 (1988).
3. J. R. Friedman, V. Patel, W. Chen, S. K. Tolpygo, J. E. Lukens, *Nature* **406**, 43 (2000).
4. A. J. Berkley *et al.*, *Science* **300**, 1548 (2003).
5. Y. Nakamura, Y. A. Pashkin, J. S. Tsai, *Nature* **398**, 786 (1999).
6. T. Duty, D. Gunnarson, K. Bladh, P. Delsing, *Phys. Rev. B* **69**, 140503 (2004).
7. D. Vion *et al.*, *Science* **296**, 886 (2002).
8. J. M. Martinis, S. Nam, J. Aumentado, C. Urbina, *Phys. Rev. Lett.* **89**, 117901 (2002).
9. I. Chiorescu, Y. Nakamura, C. J. P. M. Harmans, J. E. Mooij, *Science* **299**, 1869 (2003).
10. T. Yamamoto, Y. A. Pashkin, O. Astafiev, Y. Nakamura, J. S. Tsai, *Nature* **425**, 941 (2003).
11. C. C. Tsuei, J. R. Kirtley, *Rev. Mod. Phys.* **72**, 969 (2000).
12. L. B. Ioffe, V. B. Geshkenbein, M. V. Feigel'man, A. L. Fauchère, G. Blatter, *Nature* **398**, 679 (1999).
13. G. Blatter, V. B. Geshkenbein, L. B. Ioffe, *Phys. Rev. B* **63**, 174511 (2001).
14. A. Blais, A. M. Zagoskin, *Phys. Rev. A* **61**, 042308 (2000).
15. M. H. S. Amin *et al.*, *Phys. Rev. B* **71**, 064516 (2005).
16. M. H. S. Amin, A. Y. Smirnov, *Phys. Rev. Lett.* **92**, 017001 (2004).
17. Y. V. Fominov, A. A. Golubov, M. Y. Kupriyanov, *JETP Lett.* **77**, 587 (2003).
18. S. Kawabata, S. Kashiwaya, Y. Asano, Y. Tanaka, *Phys. Rev. B* **72**, 052506 (2005).
19. M. Tinkham, *Introduction to Superconductivity* (McGraw-Hill International Editions, New York, ed. 2, 1996).
20. A. O. Caldeira, A. J. Leggett, *Phys. Rev. Lett.* **46**, 211 (1981).
21. M. H. Devoret *et al.*, in *Quantum Tunneling in Condensed Media*, Y. Kagan, A. J. Leggett, Eds. (North-Holland, Amsterdam, 1992), chap. 6.
22. T. Bauch *et al.*, *Phys. Rev. Lett.* **94**, 087003 (2005).
23. F. M. Granozio *et al.*, *Phys. Rev. B* **67**, 184506 (2003).
24. F. Lombardi *et al.*, *Phys. Rev. Lett.* **89**, 207001 (2002).
25. R. C. Neville, B. Hoeneisen, C. A. Mead, *J. Appl. Phys.* **43**, 2124 (1972).
26. G. Burkard, D. P. DiVincenzo, P. Bertet, I. Chiorescu, J. E. Mooij, *Phys. Rev. B* **71**, 134504 (2005).
27. T. A. Fulton, L. N. Dunkleberger, *Phys. Rev. B* **9**, 4760 (1974).
28. A. Wallraff, T. Duty, A. Lukashenko, A. V. Ustinov, *Phys. Rev. Lett.* **90**, 037003 (2003).
29. J. M. Martinis, M. H. Devoret, J. Clarke, *Phys. Rev. B* **35**, 4682 (1987).
30. J. M. Martinis ***et al.***, available at http://xxx.lanl.gov/abs/cond-mat/0507622 (2005).
31. C. C. Homes *et al.*, *Phys. Rev. B* **71**, 184515 (2005).

32. This work has greatly benefited from direct inputs from S. Kubatkin. We thank the Walther-Meissner Institut for technical support. Partly supported by the European Project Quantum Complex Systems, the Swedish Foundation for International Cooperation in Research and Higher Education International Grant 2004-2075, the Swedish Foundation for Strategic Research, and the Swedish Research Council.

30 September 2005; accepted 22 November 2005
10.1126/science.1120793

Quantum Deconstruction of the Infrared Spectrum of CH_5^+

Xinchuan Huang,[1] Anne B. McCoy,[2]* Joel M. Bowman,[1]* Lindsay M. Johnson,[2] Chandra Savage,[3] Feng Dong,[3] David J. Nesbitt[3]*

We present two quantum calculations of the infrared spectrum of protonated methane (CH_5^+) using full-dimensional, ab initio–based potential energy and dipole moment surfaces. The calculated spectra compare well with a low-resolution experimental spectrum except below 1000 cm^{-1}, where the experimental spectrum shows no absorption. The present calculations find substantial absorption features below 1000 cm^{-1}, in qualitative agreement with earlier classical calculations of the spectrum. The major spectral bands are analyzed in terms of the molecular motions. Of particular interest is an intense feature at 200 cm^{-1}, which is due to an isomerization mode that connects two equivalent minima. Very recent high-resolution jet-cooled spectra in the CH stretch region (2825 to 3050 cm^{-1}) are also reported, and assignments of the band origins are made, based on the present quantum calculations.

The CH_5^+ cation was brought to the forefront of scientific interest by a range of experimental studies (*1*–*8*) and ab initio electronic structure calculations at the stationary points (*9*–*14*) that hinted at a very high degree of fluxionality owing to the unusual two-electron–three-center bonding. The large-amplitude motions displayed by CH_5^+, even in its ground state, have made spectral assignments challenging, as is evidenced by the unassigned spectrum of Oka and co-workers (*7*). Recently, a low-resolution laser-induced reaction (LIR) infrared (IR) action spectrum of CH_5^+ was reported by Asvany *et al.* (*1*). This spectrum was recorded at 110 K over a large spectral range, 540 to 3250 cm^{-1}. The LIR spectrum is a major step forward in unraveling the dynamics of this cation.

Until very recently, dynamical studies of CH_5^+ have been hampered by the lack of a full-dimensional potential energy surface (PES). Such surfaces have just appeared and have been used in a variety of classical and quantum diffusion Monte Carlo (DMC) calculations of the ground state of CH_5^+ and its isotopomers (*15*–*19*). Thus, dynamics and vibrational calculations before 2004 were carried out in a direct fashion, that is, calculating the potential and gradients "on the fly" (*20*–*23*). These pioneering calculations were done using fairly low-level density functional theory (DFT) calculations; nevertheless, they provided great insight into the fluxional nature of CH_5^+. Indeed classical, direct-dynamics DFT simulations of the IR spectrum were also reported in (*1*) at 50 and 300 K. The 300 K spectrum is in good qualitative agreement with experiment above 1000 cm^{-1}. Below 1000 cm^{-1}, intense absorption was seen in the classical spectrum but not in the experimental one, perhaps because of a lack of experimental sensitivity in that spectral region. However, it is well known that, except in the harmonic limit, classical spectra can differ substantially from quantum spectra because of the lack of quantization in the classical dynamics. Thus, while the agreement between the classical and LIR spectra above 1000 cm^{-1} was gratifying, the differences below 1000 cm^{-1} remain an open issue.

[1]Department of Chemistry and Cherry L. Emerson Center for Scientific Computing, Emory University, Atlanta, GA 30322, USA. [2]Department of Chemistry, The Ohio State University, Columbus, OH 43210, USA. [3]JILA, National Institute of Standards and Technology, and Department of Chemistry and Biochemistry, University of Colorado, Boulder, CO 80309–0040, USA.

*To whom correspondence should be addressed. E-mail: mccoy@chemistry.ohio-state.edu (A.B.M.); jmbowma@emory.edu (J.M.B.); djn@jila.colorado.edu (D.J.N.)